Air quality modeling in the city of Marrakech, Morocco using a local anthropogenic emission inventory

Lamiae Saidi, Myrto Valari, Jamal Ouarzazi

Atmospheric Environment 293 (2023) 119445

Contents lists available at ScienceDirect

Atmospheric Environment

journal homepage: www.elsevier.com/locate/atmosenv

Air quality modeling in the city of Marrakech, Morocco using a local anthropogenic emission inventory

Lamiae Saidi [a,b], Myrto Valari [a,*], Jamal Ouarzazi [c]

[a] Laboratoire de Météorologie Dynamique, Sorbonne Université, Ecole Polytechnique, IPSL, École Normale Supérieure, CNRS, Paris, France
[b] Laboratoire de Mathématiques et Dynamique de Populations, Faculty of Sciences Semlalia, Cadi Ayyad University, Marrakech, Morocco
[c] Laboratoire de chimie moléculaire, F, Faculty of Sciences Semlalia, Cadi Ayyad University, Marrakech, Morocco

HIGHLIGHTS:

- This paper, provides new information on the atmospheric composition in the greater Marrakech, Morocco region.
- We use for the first-time detailed information of anthropogenic emission in the city of Marrakech and conduct online and offline air-quality simulations over the region.
- The major component of summertime PM10 composition is dust particles, whereas in winter PM10 consists mainly of organic aerosol.
- The Atlas range blocks at some extent the import of dust plumes in the region and the export of local air-pollution to the surrounding area leading to ozone formation at high altitude.
- We show that ozone formation in the region is enhanced due to temperature increase from the absorption of infrared radiation from dust particles.

ABSTRACT

Exposure to high levels of suspended particles, and particularly dust, has been associated with increased risk of morbidity and premature mortality. The city of Marrakech is situated at a distance of only 560 km from the Sahara desert, the major dust source in the world, leading to an atmosphere rich in particulate matter all year round. In this study, we use for the first-time local scale information on anthropogenic emissions in the city of Marrakech and conduct urban-scale chemistry-transport model simulations with the CHIMERE-WRF coupled system. We compare simulated airborne particles of diameter lower to 10 μm (PM10), NO2 and O3 concentrations against surface in-situ measurements and quantify the added value of the local inventory compared to the state-of-the-art global anthropogenic emission dataset (CAMS-GLOB_ANT). We show that correlation with measurements increases and the bias decreases in all cases (pollutants, seasons and monitor sites). The major component of summertime PM10 composition is dust particles, whereas in winter PM10 consists mainly of primary organic aerosol. Comparison between simulated and observed aerosol optical depth suggests that the model reproduces accurately most of the observed summertime dust plumes. PM10 simulated concentrations are closer to in-situ surface measurements during summer than during winter with an overestimation of 13% in summer versus an underestimation of 37% in winter. Finally, we show how the Atlas range blocks at some extent the import of dust plumes in the region and the export of local air-pollution to the surrounding area leading to ozone formation at high altitude.

Modeling is an important activity to predict air-quality in Africa, where monitor networks are scarce. Our results highlight the necessity of using fine scale, local information on anthropogenic emissions to assess air-quality and in particular to (i) quantify the chemical composition of atmospheric aerosol; ii) compare the relative role of dust transport compared to locally emitted or formed suspended particles and iii) provide evidence of ozone formation at high altitude.

1. Introduction

The health cost of ambient air pollution in Morocco is estimated at an average of US$1.148 Billion, 1.05% of the country's GDP (World Bank, 2020), and was responsible for 5450 premature deaths in 2014 (Croitoru and Sarraf, 2017). WHO reported measured annual mean PM_{10} and airborne particles of diameter lower to 2.5 μm $PM_{2.5}$ concentrations in the city of Marrakech in 2012, at 58 μg/m^3 and 24 μg/m^3 (World Health Organization, 2016), which significantly exceeded the WHO guidelines concerning exposure levels of 20 μg/m^3 and 10 μg/m^3 respectively (World Health Organization, 2006). Morocco's national energy consumption relies heavily on solid fuels (wood, coal and petroleum derived products). The adverse health effects of anthropogenic pollutants are well studied. However, many studies have also shown correlation between respiratory, cardiovascular and cardiopulmonary mortality to exposure to desert dust (de Longueville et al., 2013; Giannadaki et al.,

* Corresponding author.
E-mail address: myrto.valari@lmd.ipsl.fr (M. Valari).

https://doi.org/10.1016/j.atmosenv.2022.119445
Received 11 February 2022; Received in revised form 13 October 2022; Accepted 23 October 2022
Available online 27 October 2022

2014; Morman and Plumlee, 2013).

The city of Marrakech is situated at a distance of only 560 km from the Sahara desert, the major dust source in the world. Even if the large part of the dust plumes is blocked from the Atlas range at the south of Marrakech, the atmosphere is still rich in dust particles all year round. The lack of monitor data in the region, makes air-quality modeling a necessary tool for the tracking of pollutant concentrations in Morocco and other LMICs (Low-middle income countries) in the dust-belt (Carvalho, 2016). On the other hand, anthropogenic emissions in these countries are poorly known and air-quality modeling studies use global datasets, such the CAMS-GLOBAL inventory (Granier et al., 2019) that are associated with large uncertainties and insufficient resolution for urban scale applications.

To our knowledge, there are only two recent studies that addresses urban air quality in LMIC in Africa using chemistry transport modeling (Mazzeo et al., 2022; Menut et al., 2018), but here also, anthropogenic emissions come from a global model. Most of the previous air quality modeling studies involving LMICs in Africa fall in three categories: i) evaluation of dust forecast models (Basart et al., 2012; Bouet et al., 2007; Haustein et al., 2009, 2011; Karyampudi et al., 1999; Ridley et al., 2012), none of which involve observations from urban stations; ii) evaluation of chemistry transport models at global scale, using low resolution inventories such as HTAP and CAMS in order to fully account for long range transport of desert dust across Europe or North America; iii) data collection in remote areas, such as the Saharan Mineral Dust Experiment over southern Morocco (Heintzenberg, 2009) and the Bodele Dust Experiment over the Bodele, Chad (Washington et al., 2006).

For this study, we conduct urban-scale air-quality modelling over the city of Marrakech with the WRF-CHIMERE coupled modeling system (Briant et al., 2017; Menut et al., 2021; Tuccella et al., 2019) We use an anthropogenic emission inventory provided by the Moroccan Ministry of Environment, Mines, and Sustainable Energy (MEMSD here after). The inventory contains annual fluxes for year 2013 of anthropogenic air pollutants over the entire area of the prefecture of Marrakesh split into ten anthropogenic activity sectors (SNAP). Temporal profiles for the main emission sources in the city are also provided. The MEMSD inventory, provides total emission fluxes over the Marrakech region. Using a top-down approach and spatial proxies such as the road-network, population density and the location of specific sources such as the airport we downscaled the inventory to the 2 km × 2 km mesh of the CHIMERE simulation.

This is the first application of the MEMSD emission inventory in chemistry-transport simulations. The main goal of our study is to quantify the added value of its implementation in air-quality simulations. To do so, we conducted the same simulations, using emissions from the global anthropogenic CAMS database (Granier et al., 2019), which is the state-of-the-art dataset for countries in Africa, and compared both simulations against in-situ measurements. The selection of the simulation periods is done to satisfy two constrains: i) remain close to the 2013 reference year; ii) have the maximum possible available in-situ measurements. We therefore simulated five months int the 2009–2010 winter period and four months in the 2015 summer season. To better understand the contribution of dust in the PM10 budget at the surface, we also compare the simulated 550 nm aerosol optical depth (AOD) against remote sensing observations from the ground station Saada of the AERONET network and from the MODIS instrument on board the Terra and Aqua satellites. We also discuss the chemical speciation of the simulated PM_{10} concentrations which helps understand what specific sources are omitted in the CAMS inventory. Secondary objectives of our work are to study the sensitivity of our results to activating the aerosol radiative feedback on meteorology and to increasing the vertical resolution of the model.

The paper is organized as follows: Section 2 provides all necessary information on the downscaling of the emission inventory and the model setup. Section 3 presents the model evaluation against in-situ and remote sensing observations. Our conclusions are presented in Section 4.

2. Materials and methods

2.1. Spatial and temporal downscaling of the anthropogenic emission inventory of the prefecture of Marrakech

The emission inventory provided by the Moroccan Ministry of Environment, Mines, and Sustainable Energy (MEMSD) includes annual emission fluxes for the reference year 2013 of seven air pollutants: NO_x, SO_2, NMVOC, NH_3, CO, PM_{10}, $PM_{2.5}$ and the greenhouse gas CH_4 (Moroccan Ministry of Environment, Mines, and Sustainable Energy, 2018). The MEMSD inventory is compiled following a top-down approach based on national energy consumption data and emissions factors related to each activity. Emission fluxes are provided separately for the ten SNAP anthropogenic emission sectors but are spatially averaged over the Marrakesh prefecture and therefore need to be downscaled for use in air-quality modeling. The inventory also includes temporal profiles for each of Marrakech Prefecture main emission sources:

- Agriculture
- Off-road transport
- Industry
- Residential and tertiary (including artisanal activities, Water plant, Waste treatment)
- Airport
- Railway
- Road Traffic (including a bus station)

The boundary of the map in Fig. 1 (Supplementary material) illustrates the location of the different sources accounted for in the study, (left) corresponds to the air-quality simulation domain. The boundary of the MEMSD inventory is also shown in the map (left), as well as the boundary of the census tracts, the twenty-two major axes of the road network and the surface monitor stations used for the evaluation of our simulations: two in-situ air-quality monitor stations (JEF and MHD) and the AERONET station (Saada). The location of the other main individual sources in the study domain are annotated in the zoomed area at the map on the right in Fig. 1 (Supplemntary material).

Based on traffic counting data, road traffic emissions (SNAP 7) are further divided in three parts. The first part includes emissions from the major axes of the road network, the second part emissions from secondary roads and the last part emissions from the bus station. For the downscaling of SNAP 7 emissions from the major roads and highways we identified the twenty-two major axes of the prefecture of Marrakech, at which traffic counting monitors are located. We used annually averaged daily traffic data and information on the type of vehicles on each highway for the distribution of SNAP7 emissions to the twenty-two highways (Ministry of Transport, 2013).

The second part of SNAP 7 emissions are spatially distributed to the twenty census tracts of the region based on population density. Finally, emissions from the bus station are allocated to the corresponding area. Other major emission sources in the region include several industries, an artisan zone, the railway station, a waste treatment area, the water plant, and the airport. As for the bus station, we first identified the coordinates of the polygons defining each geographic zone and then spatially allocated these surface emissions on the polygons. Residential/tertiary (SNAP 2) emissions and agricultural (SNAP 10) emissions are spatially distributed to the different census-tracts of the region based on population density. Fig. 2 (Supplementary material) shows the result of the spatial allocation of residential (SNAP 2) and road-transport (SNAP7) PM10 emission fluxes in the census tracts and the road network of the prefecture of Marrakesh.

As a next step, the MEMSD inventory in mapped to the 2 km × 2 km resolution mesh of the air-quality simulation as shown in Fig. 1 (right columns) for NO_2 and $PM_{2.5}$. Fig. 1 also compares emission fluxes obtained with the described methodology (MEMSD) against the global

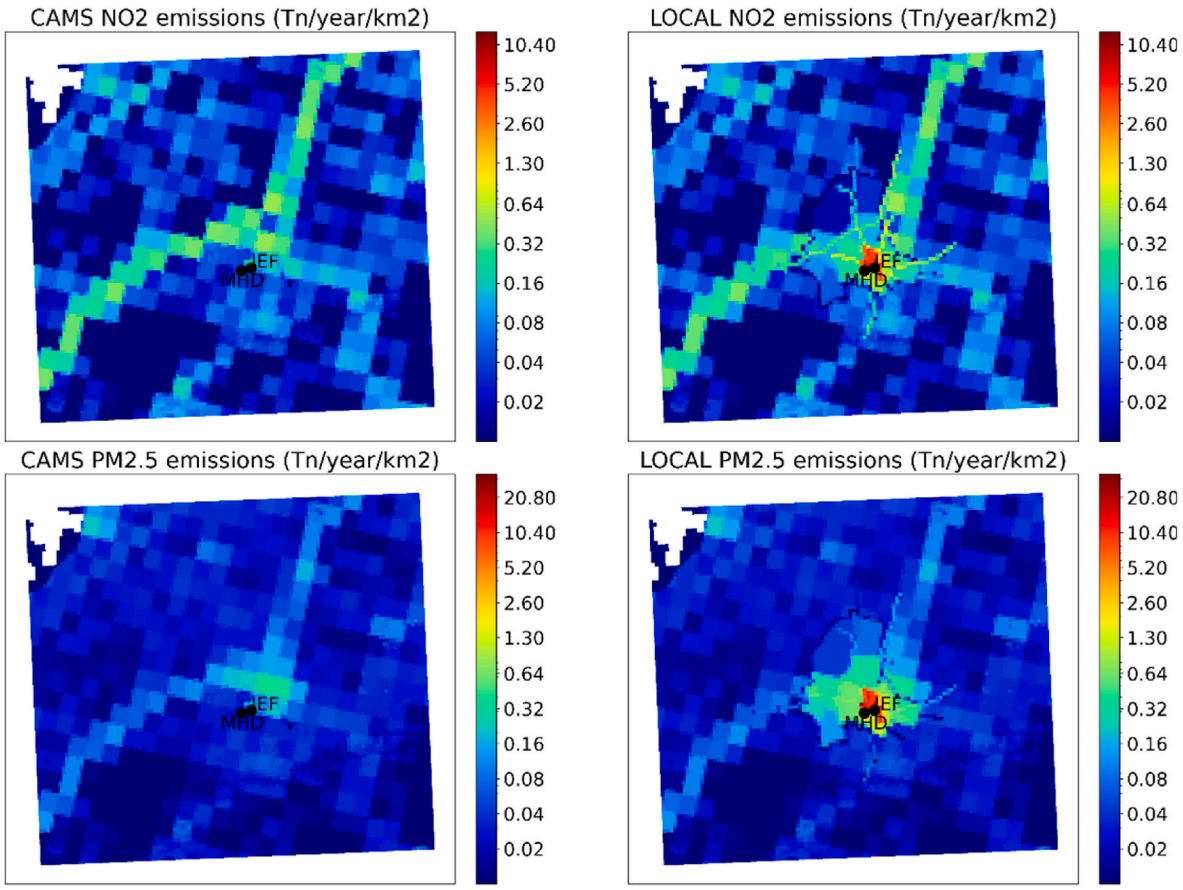

Fig. 1. (Left) Annual emission fluxes (2013) of the global anthropogenic CAMS inventory (Granier et al., 2019) downscaled to the 2 km × 2 km resolution CHIMERE simulation mesh. (Right) Combination of the CAMS and MEMSD (local) inventories to compose the emission fluxes used in the CHIMERE simulations. The top row shows maps of NO_2 emissions, the bottom map emissions for $PM_{2.5}$.

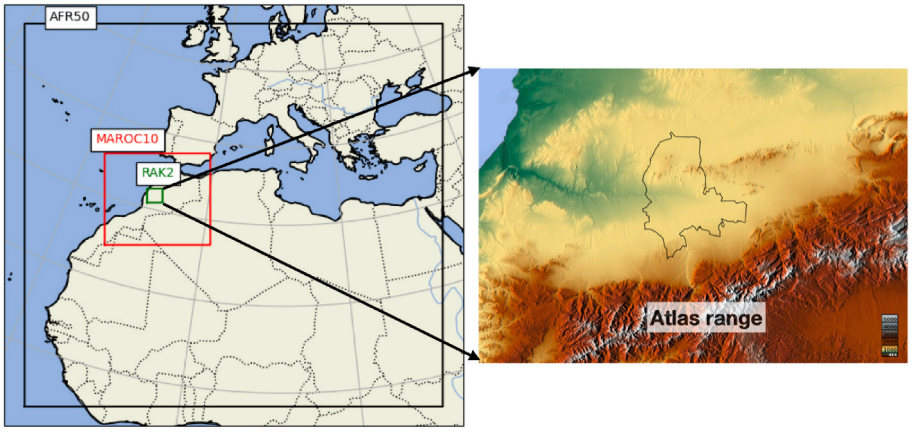

Fig. 2. The three-level nesting with grid ratio of five (left). Zoom in the inner RAK2 domain showing the Atlantic coastline at the north-west and the Atlas Range at the south-east. The black-line boundary in the center of the map shows the boundary of the Marrakesh district. The relief map on the right is made with © Google Earth version 2019.

CAMS anthropogenic emission inventory (Granier et al., 2019). The road network is finely resolved in the maps of NO_2 and at a certain degree $PM_{2.5}$ emissions. Also, the densely populated city center in clearly distinguished from the suburbs reflecting the population density horizontal gradients. These spatial features are not resolved in the CAMS inventory. Since the MEMSD inventory covers only a small area of the simulation domain we used emission fluxes from the global CAMS anthropogenic emission inventory in grid-cells outside of the prefecture of Marrakesh. A similar approach has been followed in the work of (Mazzeo et al., 2018) in Santiago, Chili.

Fig. 3 (Supplementary material) shows the contribution of each activity sector to the total annual emissions of the two anthropogenic inventories discussed in this study, the global CAMS inventory which is assumed as the reference inventory and the local MEMSD inventory. Based on the MEMSD inventory, the main source of PM_{10} and $PM_{2.5}$ emissions is residential/tertiary combustion (75% and 83%,

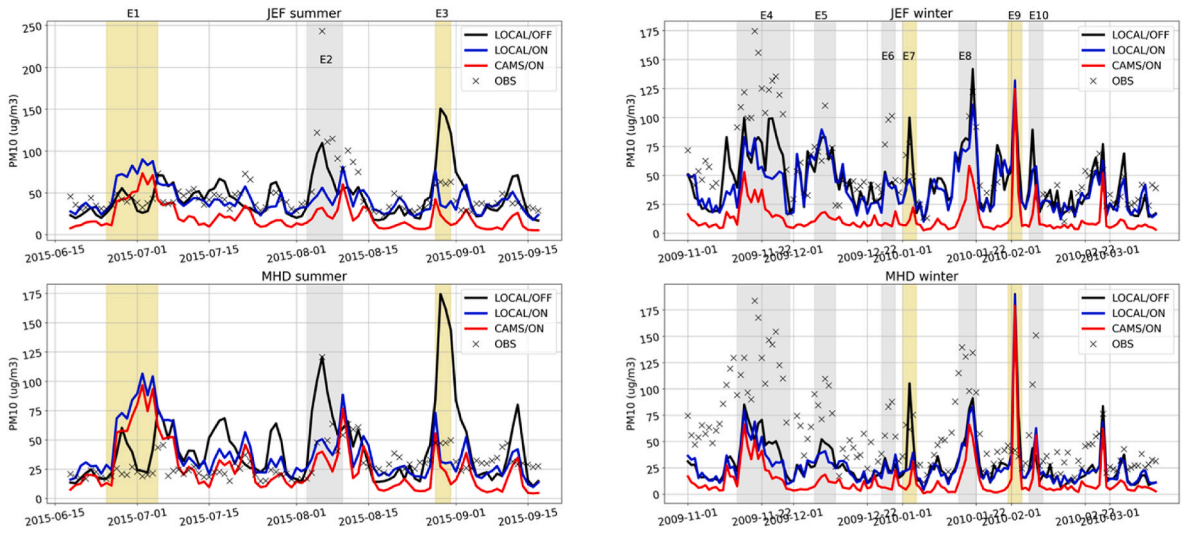

Fig. 3. PM_{10} daily averaged concentrations for the summer period (left panels) and winter period (right panels) at the two in-situ monitor sites: urban site (JEF) on the top row and rural site (MHD) on the bottom row. Shadowed areas correspond to concentrations over the 100 μg/m3 threshold, they are grey when the threshold is reached by the observations and yellow when it is only reached by the simulations. (For interpretation of the references to colour in this figure legend, the reader is referred to the Web version of this article.)

respectively), followed by road transport (12% and 13%, respectively). NO_x road transport contributes at almost 50% and another 31% comes from agriculture. The residential/tertiary sector has a contribution of 13%. The major source of COVNM is road transport (28%), closely followed by the residential sector (22%) and combustion in the manufacture industry (23%), residential combustion (22%). Another 10% comes from waste treatment. Comparing the CAMS and MEMSD inventories, we see that according to CAMS emissions the industrial activity in the region is much higher, leading to much higher emission fluxes for SO_x. The industrial sector also has a significant contribution in particle emissions in the CAMS inventory, whereas the major contributor of PM following the MEMSD local inventory is the residential sector. Primary aerosols, CO and NO_x emissions are much higher in the MEMSD inventory (almost two times higher). The CAMS inventory prescribes much higher NH3 fluxes, mainly from agricultural activity. Non-volatile organic compounds are also significantly higher in the CAMS inventory and their mains source is solvent use. The fact that the local MEMSD emission inventory has much higher NOx emissions and much lower VOC emissions is bound to lead to an ozone formation driven by a more COV-limited regime compared to the simulation using CAMS emissions.

The annual MEMSD fluxes were temporally downscaled to hourly fluxes based on sector-dependent emission profiles provided along with the inventory. The procedure follows three steps: i) annual emissions are distributed across the twelve months of the year (left panels of Fig. 4 Supplementary Material); ii) weekly profiles are applied to represent the day-of-week variability (middle panels of Fig. 4 Supplementary Material) and iii) hourly profiles represent the diurnal cycle of emissions (right panels of Fig. 4 Supplementary Material) profiles. Comparing the temporal profiles between the MEMSD and CAMS inventory we find large discrepancies. The seasonal cycles of agriculture activity are out of phase with the MEMSD inventory having maximum agriculture emission during the summer months when CAMS emissions are relatively low. Also, the CAMS inventory has a strong seasonal cycle for residential emissions with low emission during summertime and high emission

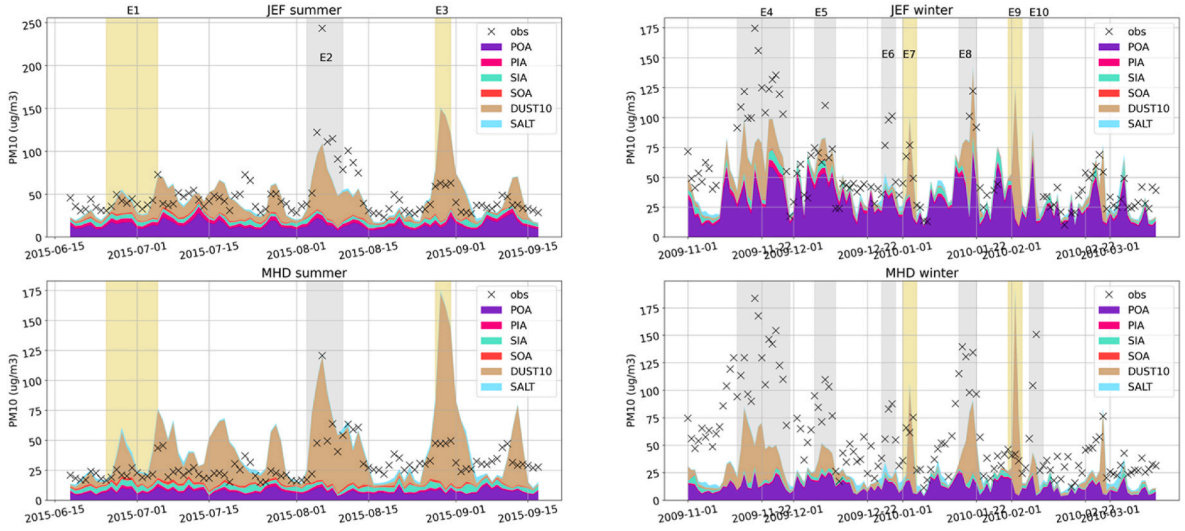

Fig. 4. Daily average modeled (filled lines) and observed (crosses) PM_{10} concentrations during the summer months (left) and winter months (right) at the urban JEF (top) and rural MHD (bottom) monitor stations. Color fills at each model line correspond to different chemical species of the PM10 composition. Simulations use the local MEMSD inventory of anthropogenic emissions. (For interpretation of the references to colour in this figure legend, the reader is referred to the Web version of this article.)

during winter whereas the MEMSD inventory has the same emissions all year long. The local MEMSD inventory also shows a peak in road-transport emissions in August, corresponding to the tourist season. The traffic rash hours are also different depending on the inventory. Following the MEMSD local inventory rash hours occur at 12:00 and 17:00 GMT whereas according CAMS they occur at 8:00 and 20:00 GMT. These remarks highlight some important benefits related to the use of a local inventory, namely considering local specificities, habits and customs such as residential heating practices, application of agricultural fertilizers or working hours.

2.2. The WRF-CHIMERE modeling system

The v2020r1 release of the coupled WRF-CHIMERE model (Menut et al., 2021) is used for all meteorological and air-quality simulations of the study. Two different simulations will be discussed: 1) the OFF case where meteorology is used as input for the chemistry-transport calculations and 2) the ON case with online interactions between CHIMERE and WRF by considering the aerosol direct and indirect radiative effects on meteorology.

The goal of our study is to quantify the benefit of using a local emission inventory for modelling air-quality at the urban scale at the greater Marrakesh area. For this reason, we simulate pollutant concentrations at an area of 220 km (west to east dimension) x 200 km (south to north dimension) centered around the city of Marrakesh. The Marrakesh-Safi region and the Atlantic coastline are at the north-west of the domain and Morocco's High Atlas range with peaks up to 4000m is found at the southern-east part of the domain (Fig. 2 right). The horizontal resolution of the simulation domain, called RAK2 hereafter, is of 2 km × 2 km. We use three-levels of nesting with a grid-ratio of five to obtain accurate pollutant concentration at the urban scale as shown in Fig. 2 (left). The bigger domain at 50 km × 50 km resolution (AFR50) includes the Sahara Desert on the south, important source of dust during the summer period, the entire Mediterranean Sea and the largest part of Europe. In this manner, most natural and anthropogenic sources of air-pollution that may reach the Marrakesh district and affect local air-quality are included in the simulation. An intermediate domain of 10 km × 10 km (MAROC10) is used covering the north Morocco and a small part of the southern Iberian Peninsula.

Gas and aerosol boundary conditions for the AFR50 domain come from LMDz-INCA global simulations (Hauglustaine et al., 2014). For dust, boundary conditions are taken from the GOCART model (Ginoux et al., 2004). For the two nested domains, hourly boundary conditions are taken from the parent domain. Biogenic emissions are calculated online with the MEGAN model embedded in the WRF-CHIMERE system (Guenther et al., 2006). Forest fire emissions were not included in our simulations due to the arid nature of the studied region. Sea salt fluxes are calculated, according to (Monahan et al., 1986). Mineral dust emissions are calculated using the parametrization of (Marticorena and Bergametti, 1995) for saltation and the dust production model for sandblasting (Alfaro and Gomes, 2001) with optimization following (Menut et al., 2005). These calculations are based on land-use data from the STATSGO-FAO soil dataset, and the USGS (United States Geological Survey) land-use dataset at high horizontal resolution.

Anthropogenic emissions outside the Prefecture of Marrakesh were taken from the global CAMS anthropogenic emission inventory at a resolution of 0.1° × 0.1° (Granier et al., 2019). Emissions in the inner most domain (RAK2) and inside the Prefecture of Marrakesh are taken from the local MEMSD inventory as described in Section 2.1.

In the present study we present results of three different simulations:

- LOCAL/ON: This simulation uses the MEMSD emissions inside the Prefecture of Marrakesh and also online interactions between chemistry and meteorology to take into account the direct and indirect effects of aerosols on radiation. This simulation has a high vertical resolution of thirty vertical layers from surface up to 200 hPa.
- CAMS/ON: This simulation is identical to the LOCAL/ON in all aspects apart from the input anthropogenic emission fluxes. In this simulation emissions over the entire RAK2 domain are taken from the global CAMS anthropogenic emission inventory. This simulation is directly comparable to the LOCAL/ON simulation and allows to quantify the added value of the use of the local MEMSD inventory.
- LOCAL/OFF: This simulation uses the local MEMSD emission inventory inside the Prefecture of Marrakesh but no feedback of chemical concentrations on meteorology is taken onto account. Also, the vertical resolution is coarser than the ON simulations, with fifteen vertical layers from surface up to 200 hPa, typically used in regional simulations.

The High Atlas range in the south of the RAK2 domain acts as a barrier for dust particles emitted from the Sahara Desert to enter the simulation domain. A high resolution of the vertical transport is important to correctly simulate the import of Saharan dust. Comparing the results of the LOCAL/OFF with the LOCAL/ON simulation gives some insight on the impact on surface pollutant concentrations of the i) radiative interactions between aerosols and atmospheric dynamics and; ii) vertical resolution.

The three simulations, LOCAL/OFF, LOCAL/ON and CAMS/ON, were run for the winter and summer periods of the study:

- Winter period: from November 1, 2009 to 15 March 2010.
- Summer period: from 15 June 2015 to 30 September 2015.

3. Results

3.1. Model evaluation based on statistical metrics

Model performance was assessed through statistical parameters that compare PM_{10}, O_3 and NO_2 modeled concentrations to observed concentrations at JEF and MHD in-situ monitors for each of the two simulation periods. The statistics used were: pearson correlation coefficient (r), mean bias error (MBE), normalized mean bias (% NMB) and the root mean square error (RMSE), maximum daily 8hr average for ozone (MDA8), which are common forms of the current WHO Ambient Air Quality Standards and among most measurement networks (Emery et al., 2017).

For the model evaluation that follows we use in-situ observations from two monitor sites, the JEF station, located in the urban tissue of the city of Marrakesh and the MHD station, located at the outskirts of the city. The model grid-cells exposed to Anthropogenic emissions due to road transport and residential combustion in the simulation grid-cell including the urban station JEF are more than two times higher than emissions at the grid-cell including the rural station MHD according to the local MEMSD inventory (not shown). We also compared simulated aerosol optical depth (AOD) values with local-scale AOD data from the Saada station of the Aerosol Robotic Network (AERONET: https://aeronet.gsfc.nasa.gov/) and regional-scale (10K) AOD measurements from MODIS Terra (https://doi.org/10.5067/MODIS/MOD04_L2.061) and Aqua (https://doi.org/10.5067/MODIS/MYD04_L2.061) level 2 aerosol products.

3.1.1. Particulate matter

Since the in-situ measurements available in the region measure only the coarser part of suspended particles (PM10), our model evaluation focuses on particles of diameter lower or equal to 10 μm.

Simulated PM10 concentrations are comparable between the two seasons with summertime levels being slightly higher than wintertime levels due to higher anthropogenic emissions in the summer (tourist season) and also more frequent dust emission in the Sahara Desert and transport across the Atlas range at the south of the domain. As shown in

Table 1
Scores on daily averaged PM_{10} concentrations at JEF (urban) and MHD (rural) monitor sites for the two periods of the study.

Summer 2015						Winter 2009/2010					
	Site	MBE (μg/m^3)	r	RMSE (μg/m^3)	NMB(%)		Station	MBE (μg/m^3)	r	RMSE (μg/m^3)	NMB(%)
LOCAL/OFF	JEF	−2.40	0.54	26.16	−5.10	LOCAL/OFF	JEF	−12.66	0.77	25.02	−22.77
	MHD	10.56	0.50	28.37	33.69		MHD	−30.12	0.50	44.81	−50.47
	ALL	5.25	0.55	24.77	13.66		ALL	−21.17	0.78	30.94	−36.96
LOCAL/ON	JEF	−5.67	0.25	29.66	−12.03	LOCAL/ON	JEF	−17.40	0.68	30.28	−31.30
	MHD	4.78	0.12	24.51	15.25		MHD	−32.65	0.46	47.02	−54.73
	ALL	0.69	0.22	24.84	1.80		ALL	−24.95	0.73	35.68	−43.55
CAMS/ON	JEF	−26.48	0.25	38.94	−56.21	CAMS/ON	JEF	−44.14	0.69	52.21	−79.40
	MHD	−6.62	0.11	24.84	−21.10		MHD	−45.85	0.40	57.72	−76.83
	ALL	−15.32	0.21	28.84	−39.82		ALL	−45.08	0.67	53.44	−78.69

Table 1, the model overestimates summer concentrations (NMB 14%) and underestimates winter concentrations (NMB -37%). Pearson correlation coefficients in the daily mean values is 0.55 in summertime and 0.78 in wintertime. The LOCAL/OFF simulation meets the goals that the majority of models have achieved $r > 0.4$ (Emery et al., 2017) and is as good as European studies using yearly updated EMEP inventories ($r = 0.6$ (Gama et al., 2020),).

These results are comparable to the results presented in Menut et al. (2021) even if the simulations presented there where run at a much coarser model resolution (60 km × 60 km). These results also concur with Im et al. (2014) AQMEII phase 2 study on particulate matter, comparing eight online coupled air quality models that also showed strong underestimation of PM_{10} concentrations by up to 57%, with the largest biases occurring in the winter period by up to 85%.

Looking separately at the urban (JEF) and rural (MHD) stations we see that according to the in-situ observations, during the winter period, both stations have very similar daily averaged PM10 concentration levels whereas during summertime PM10 concentrations at the urban (JEF) station are significantly higher than those in the rural station (MHD). These differences are most probably explained by a combination of two factors: i) according to the MEMSD inventory anthropogenic PM10 emissions are almost three times higher in the vicinity of the urban station JEF compared to MHD (not shown) and this difference is more pronounced during the summer months (double peak due to the tourist season and agricultural activity) ii) in winter, higher winds lead probably to enhanced PM10 concentrations due to erosion of arid soil and local emission or resuspension of dust. This emission source is bound to affect more the rural station than the urban center.

The model does not reproduce this spatial and seasonal variability. The model does not see any local dust emission inside the RAK2 domain (not shown) and therefore, the difference between simulated PM10 concentrations between the urban and rural sites for both seasons directly reflects the difference in the PM10 anthropogenic emissions between the two sites and differences in meteorology. Also, modeled concentrations are higher during the summer period than in wintertime for two different reasons: i) higher anthropogenic emissions in summertime (tourist season and enhanced agricultural activity) and; ii) more frequent dust storms at the Sahara Desert with a synoptic circulation favorable of an import of dust particles inside the RAK2 domain.

The CHIMERE model simulation with emissions from the local MEMSD inventory and without aerosol radiative feedback (LOCAL/OFF) accurately simulates summertime PM_{10} concentrations at the urban site (JEF) with a low underestimation of 5% (NMB). The underestimation of PM10 concentrations is higher during the winter period 23%. At the rural (MHD) site the model overestimates PM10 concentrations by 33% in summertime and underestimates them by 36% during winter. The overestimation of surface PM10 concentrations over the rural site during summer may be related to insufficient vertical resolution bringing too much dust particles from higher layers to the ground during dust events. This is more pronounced over the rural areas with thicker boundary layers where upper level air, rich in dust particles, gets mixed with the surface layer. This point is supported by the comparison between LOCAL/OFF simulation and the LOCAL/ON (fifteen versus thirty vertical layers respectively). The summertime overestimation of PM10 concentrations drops from +33.69% in the LOCAL/OFF to +15.28% in the LOCAL/ON simulation. The underestimation of PM10 concentrations at the rural site during winter, which persists no matter the model's vertical resolution, is probably due to the absence of local emissions of particles due to wind erosion and resuspension process in the model. It is less plausible that the bias stems from the anthropogenic inventory since it only affects wintertime concentrations at the rural site.

Even if a one to one comparison between the LOCAL/OFF and LOCAL/ON simulations is not possible since other model parameters are different between the two model set-ups (vertical resolution) we qualitatively present certain observations. Model results with and without considering aerosol radiative feedback on meteorology are rather similar in winter time (Pearson correlation and bias are of the same order of magnitude). In summertime, the bias in the online simulation is significantly lower (in particular at the rural site) than in the offline simulation but the correlation in the online simulation is much lower (0.22 vs. 0.5). However, looking at the time-sires in Fig. 3 we see that the decrease in the summertime correlation comes from two isolated events: i) a falsely simulated peak in the end of June beginning of July 2015 (E1 in Fig. 3) and; ii) the underestimation of the peak in the first week of August (E2 in Fig. 3). The rest of the simulated summer period the online simulation (LOCAL/ON) seems to provide good PM10 concentration predictions and accurately reproduce the observed daily variability. However, we are not able to tell if these discrepancies between the LOCAL/ON and LOCAL/OFF simulations stem from the online coupling or the finer model vertical resolution in the online simulation.

In wintertime, we observe much more frequent peaks in PM10 observed concentrations (episodes marked as E4, E5, E6, E8 and E10 in Fig. 3) that are, in most cases, seen by the CHIMERE simulation but systematically underestimated. Shadowed areas in Fig. 3 correspond to days where observed or modeled simulations are above the 100 μg/m3 threshold at least one of the two monitor site locations. The model simulates the peak in the end of November 2009 (episode E4) even if it underestimates it significantly. The observed peak at the end of December 2009 (E6) is missed by the CHIMERE model. The three peaks at the second week of December (E5), the first week of January (E7) and the second week of February (E10) are quite well simulated even if most of the time underestimated or not well localized. For example, the February peak (E10) is simulated at the location of urban (JEF) site but the in-situ observations record it over the rural site (MHD). The model simulates a peak in PM10 concentrations in the beginning of February (E9) that is not recorded at the MHD station (no data available over the JEF monitor). We note here, that (Kong et al., 2015) WRF-Chem simulations with only direct effects of aerosols or no aerosols feedback performed better than simulations including both direct and indirect effects. This remark may suggest that the representation of aerosol indirect effects needs to be improved in online coupled models. The underestimation of dust concentrations in CHIMERE-WRF simulations has also been discussed in (Gama et al., 2020) for Portugal.

If we now compare the LOCAL/ON simulations with the CAMS/ON

simulation based on both Table 1 and Fig. 3 we find a large improvement in the model bias with the use of the local MEMSD inventory. PM10 winter concentration are underestimated by 79% with the CAMS inventory during winter and by 43% with the local MEMSD (averaged across both sites). During summer, simulations using CAMS emissions lead to PM10 underestimation by 40% whereas the use of the local MEMSD inventory leads to a slight overestimation by 0.7%. Looking at the time-series of Fig. 3 we see that PM10 concentrations modeled with the CAMS inventory are always below PM10 concentrations modeled with the local MEMSD inventory directly pointing to a deficit in primary particulate matter in the anthropogenic inventory.

Looking at the chemical composition of PM10 (Fig. 4) we see that in wintertime, most of the PM_{10} mass is primary organic aerosol with contribution of 63% at the urban (JEF) site and 42% at the rural site (MHD). In summertime dust particles represent most of the modeled PM10 mass. The other components have more or less constant contribution to the modeled PM10 mass regardless the season or the monitor site. . We clearly see that modeled summertime PM10 is almost all the time dominated by dust particles at both urban and rural locations. We see that the very accurate simulation of the beginning of August event (E2), especially over the rural station (MHD) represents a dust event for the model. The simulated dust peak at the end of August (E3) is present, but much lower in the surface in-situ observations. During winter, simulated PM10 concentrations are mainly composed of primary emitted particles except from sporadic dust events, namely the November event (E4), the beginning of December episode (E5), the two January peaks (E7 and E8) and the February episodes (E9 and E10). In some cases, the observed peak values are underestimated in the model, with maximum underestimation observed during the November 2009 E4 event (65%) and the E10 events (MHD location). In other cases, the model prediction is quite accurate such as during the E7 and E8 (JEF) events. In general, the bias is rather small at the urban site (JEF) but high at the rural site (MHD).

To help understanding the nature of PM10 pollutant episodes in the area during the two simulation periods we extracted local-scale aerosol optical depth (AOD) data from the Saada station of the Aerosol Robotic Network (AERONET: https://aeronet.gsfc.nasa.gov/) and regional-scale (10K) AOD measurements are taken from MODIS Terra (https://doi.org/10.5067/MODIS/MOD04_L2.061) and Aqua (https://doi.org/10.5067/MODIS/MYD04_L2.061) level 2 aerosol products. We also show the simulated AOD values, calculated with the Fast-J code embedded in CHIMERE. Fig. 5 shows time series of simulated and observed aerosol optical depth (AOD) during the summer and winter periods of the simulations. Terra and Aqua satellite trajectories intersect the model domain twice a day between 10am and 12pm UTC. Daily AOD simulated and AERONET values in the time-series of Fig. 5 correspond to hourly averaged values within the 10am to 12pm time-range.

The AOD time-series confirm a severe dust episode in the beginning of August (E2), with very high values of AOD (>2). This episode is reflected in the PM10 concentrations at both in-situ monitor locations and is also simulated by the model. A second much less severe peak in AOD time series (almost 1) is observed by the MODIS instrument during the summer period at the end of August 2015 (no AERONET measurement available). This peak, corresponds to the E3 event discussed above and is also seen in the in-situ observations. Simulations overestimate PM10 concentrations during this episode even if the simulated AOD is significantly underestimated. The absence of peak in observed AOD during the E1 episode confirms that the simulation is mistaken here. Observed AOD values during winter are most of the time below 0.4 except for two episodes: the E4 episode at the second part of November 2009 and the E10 episode at the beginning of February. These two episodes may be dust events. Both these events are also seen by the in-situ observations and simulated by the model albeit significant underestimation. The low AOD values outside these episodes suggest that other sources of PM10

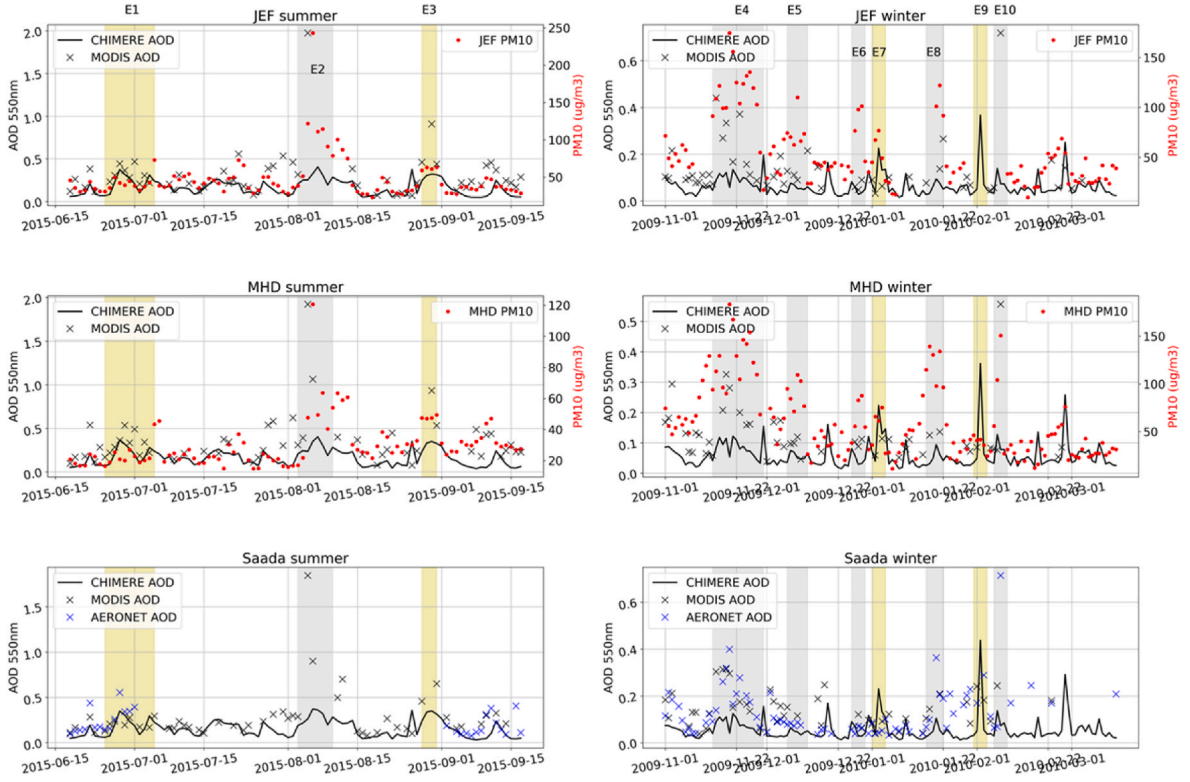

Fig. 5. Daily time series of the aerosol optical depth (AOD) at 550 nm, averaged from 10am to 12pm UTC simulated with the fast-J code embedded in CHIMERE (black line), measured with the MODIS instrument on-board the Terra and AQUA satellites (black crosses) and the lidar at the ground station Saada of the AERONET network (blue crosses). Red circles correspond to in-situ measurements of PM10 concentrations (y-axes on the right of the graphs) at the same time occurrence. (For interpretation of the references to colour in this figure legend, the reader is referred to the Web version of this article.)

pollution act in wintertime rather than dust storms at the Sahara Desert. The fact that the model underestimation of PM10 observed concentrations affects particularly (if not only) the rural (MHD) location suggests that the source of the bias is probably not the anthropogenic inventory but rather the absence of local sources of PM10 particles in the vicinity of the rural area. As mentioned above, this is most probably the absence of local dust sources in the arid area around the MHD station.

Table 1 (Supplementary material) gives the number of days of exceedance of the WHO guidelines threshold in each of the simulation months. The model reproduces quite well the exceedances at the urban location (JEF). On the contrary, the wintertime model underestimation of PM10 concentrations over the rural area is clearly reflected in the table. Also, significant overestimation of the number of exceedances is simulated at the proximity of the rural station (MHD), particularly in July. This overestimation corresponds to dust events and as suggested before may be explained by the insufficient vertical resolution that over the relatively thick boundary layer over the rural stations brings too much dust to the ground.

Maps of monthly averaged, simulated dust concentrations are shown in Fig. 5 (Supplementary Material). The Sharan desert storms during the summer months are clearly seen in the dust maps as well as the High Atlas Mountain range in the south of the domain, blocking the import of dust particles in the RAK2 domain.

3.1.2. Nitrogen dioxide

During the winter period observed 24-hr average NO_2 concentrations are very similar at the two monitor sites (10 ppb at the urban site JEF and 11 ppb at the rural site MHD). NO2 simulations are much higher during summer at both stations, due to higher anthropogenic emissions during the tourist season and enhanced agricultural activity. The simulations do not reproduce the difference between winter and summer concentrations. Also, modeled NO2 concentrations at the urban station JEF are always higher than at the rural station (MHD) directly reflecting differences in anthropogenic emissions. The model underestimates summertime NO_2 concentrations and overestimates NO2 wintertime concentrations. As shown in Fig. 6, simulations using the CAMS inventory provide extremely biased NO2 concentrations with a constant underestimation reaching up to 95% (Table 2). This bias is much more

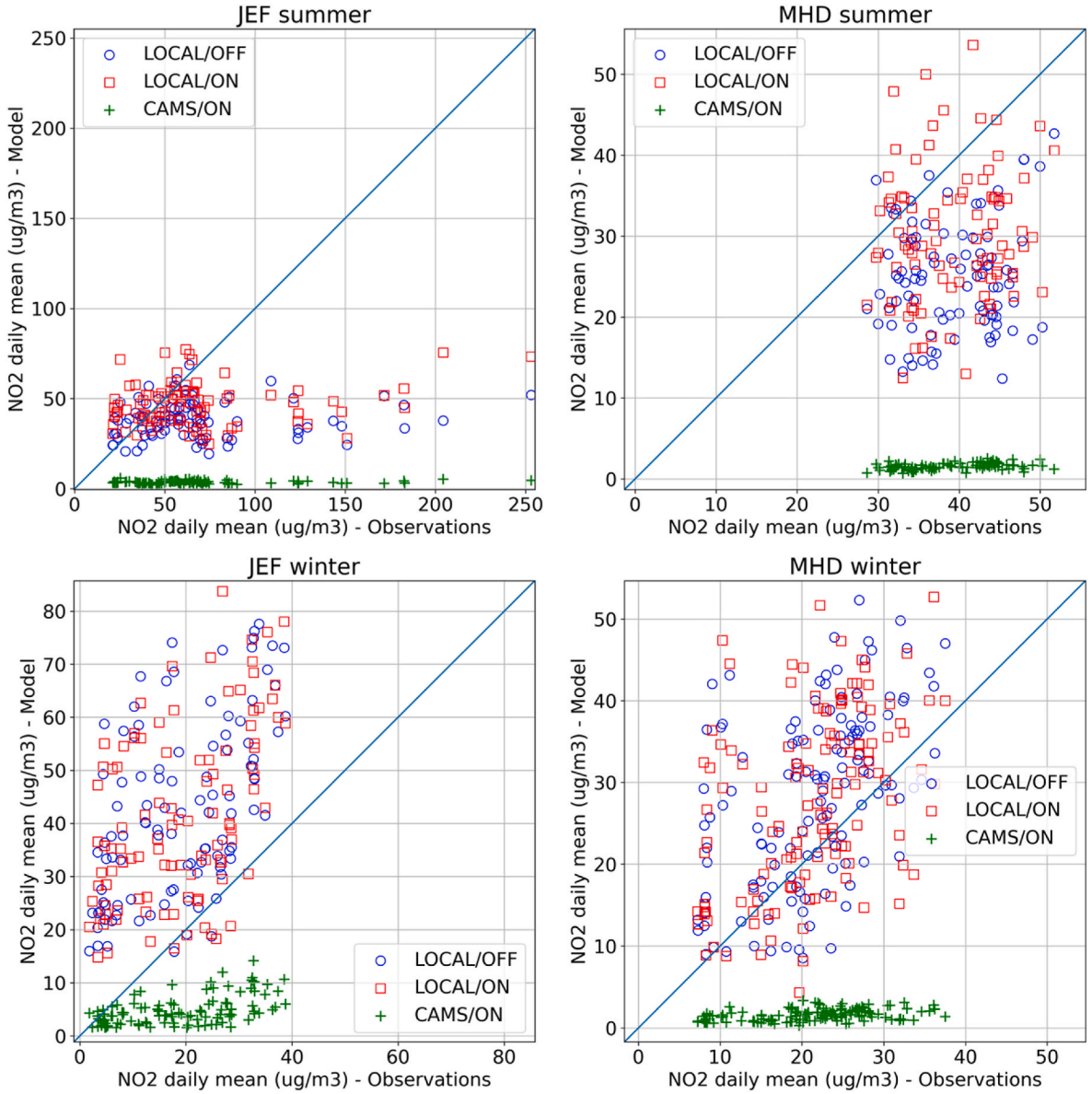

Fig. 6. Scatter plots of modeled versus observed daily averaged NO_2 concentrations at summer (top) and winter (bottom) months over the urban JEF (left) and rural MHD (right) monitor sites. Different signs correspond to different simulations LOCAL/OFF, LOCAL/ON and CAMS/ON.

Table 2
Daily averaged NO_2 concentration scores at the urban (JEF) and rural (MHD) monitor sites during the summer and winter simulation periods.

Summer 2015						Winter 2009/2010					
	Site	MBE (ppb)	r	RMSE (ppb)	NMB(%)		Station	MBE (ppb)	r	RMSE (ppb)	NMB(%)
LOCAL/OFF	JEF	−14.70	0.12	27.09	−40.28	LOCAL/OFF	JEF	13.31	0.50	15.41	132.64
	MHD	−6.28	0.13	7.90	−30.46		MHD	4.11	0.51	6.64	36.26
	ALL	−10.66	0.21	16.00	−37.20		ALL	9.08	0.61	10.70	87.84
LOCAL/ON	JEF	−10.02	0.19	24.58	−27.44	LOCAL/ON	JEF	12.58	0.45	15.06	125.36
	MHD	−3.55	0.11	6.40	−17.21		MHD	3.95	0.44	6.72	34.86
	ALL	−6.84	0.14	14.30	−23.88		ALL	8.82	0.55	10.70	85.27
CAMS/ON	JEF	−34.46	0.12	41.21	−94.41	CAMS/ON	JEF	−7.43	0.44	9.10	−74.05
	MHD	−19.76	0.34	19.97	−95.72		MHD	−10.49	0.39	11.16	−92.46
	ALL	−27.20	0.11	29.71	−94.89		ALL	−8.60	0.54	9.41	−83.17

pronounced than in the case of PM10 underlying the importance of the anthropogenic inventory for NO2. Wintertime NO2 modeled concentrations overestimate significantly the observed NO2 levels, especially at the urban (JEF) monitor site. The online coupling with meteorology and the increase un model vertical resolution do not seem to change model performance. Model predictions are better during the summer months especially over the urban monitor site (JEF). The model underestimates the high NO2 peaks, which is expected given its 2 km × 2 km horizontal resolution. However, the underestimation of observed summertime NO2 peak concentrations decreases with the LOCAL/ON simulations compared to the LOCAL/OFF simulations (LOCAL/OFF -37% vs. LOCAL/ON -24%). This improvement is most prominent at the rural (MHD) site. It is most probably due to the increased vertical resolution in the online simulations resulting in a more realistic vertical transport of surface emissions. However, as in the PM10 case, the pearson correlation decreases in the LOCAL/ON simulations compared to the LOCAL/OFF. This is probably due to the radiative feedback of aerosol concentrations on dynamics (mainly temperature and wind fields).

Fig. 6 (Supplementary Material) shows the diurnal cycle of observed and modeled NO2 concentrations. We see that not only the emitted mass and the spatial distribution is improved with the MEMSD inventory compared to the CAMS emissions but also the temporal profile. This remark, highlights the importance of using local information concerning anthropogenic emissions since they reflect up to a certain extent local habits and customs.

3.1.3. Ozone

Over the urban station (JEF) the simulations using emissions from the local MEMSD inventory reproduce quite well observed ozone concentrations (Fig. 7). We show that the LOCAL/ON simulation with radiative feedback of aerosols on meteorology leads to overestimation of ozone concentrations (see also Table 3). As discussed

Table 3
Scores of 8h maximum daily average O_3 concentrations (ppb) at JEF, MHD stations and both stations averaged in Summer (2015).

Summer 2015					
	Site	MBE (ppb)	r	RMSE (ppb)	NMB(%)
LOCAL/OFF	JEF	6.23	0.36	10.23	16.26
	MHD	23.34	0.50	24.58	91.10
	ALL	15.21	0.46	16.95	48.87
LOCAL/ON	JEF	7.53	0.24	17.14	19.66
	MHD	26.10	0.34	30.14	101.80
	ALL	16.90	0.33	22.24	54.37
CAMS/ON	JEF	21.25	0.28	27.26	55.52
	MHD	31.78	0.35	35.64	123.93
	ALL	26.63	0.36	31.02	85.66

in section 2.3.1, during summertime the atmosphere is rich in dust particles. Dust particles absorb radiation and heat the atmosphere leading to enhanced ozone formation compared to the simulations not accounting for aerosol radiative feedback on meteorology (Briant et al., 2017). Correlation between modeled and observed ozone concentrations at the rural station (MHD) is compared to the urban station JEF. This shows that photochemical ozone built-up is fairly simulated. However, the bias is higher at the rural station: the model seems to form too much ozone downwind, and the plume is located too close to the city-center. With only one urban and one rural monitor site it is impossible to further investigate into these assumptions. The high bias in ozone concentrations may be due to errors in the emission of its precursors (NOx and VOC) and also to errors in wind speed and direction which would explain the mislocation of the ozone plume. The bias may also stem from errors in the spatial allocation of emissions, with too sharp horizontal gradients. NOx emissions decrease by more than half in the 12 km distance from the JEF to the MHD station. Having said this,

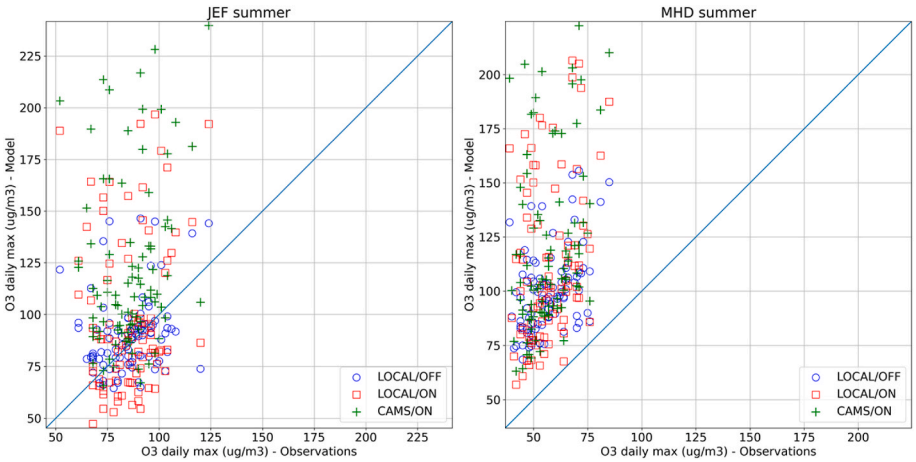

Fig. 7. Scatter plots of summertime modeled versus observed daily maximum ozone concentrations at over the urban JEF (left) and rural MHD (right) monitor sites. Different signs correspond to different simulations LOCAL/OFF, LOCAL/ON and CAMS/ON.

ozone concentrations modeled with the local MEMSD inventory are much closer to the measurements compared to simulations using the CAMS anthropogenic inventory. With CAMS emissions, ozone concentrations are highly overestimated.

The map at the top left panel of Fig. 8 shows summertime average (July and August) daily averaged ozone concentrations. We see that an ozone plume is formed at the south of the city of Marrakech. The prevailing surface wind has a north-south direction bringing polluted air from the city at the south. As the air masses reach the Atlas range at the south of the domain they are forced to elevate at higher atmospheric layers. As shown in the right top panel of Fig. 8 the ozone plume extends up to the fifth model layer at about 2000m above sea level. The bottom panel of Fig. 8 shows a vertical transect from surface level up to the 15th model vertical layer (above 5000m above sea-level). Once the ozone plume reaches the mountain, it is transported back towards the north under the force of the katabatic mountain winds. We see in this transect, that ozone is formed downwind at different levels above the ground. A similar process has been observed in the ozone plume over the Santiago, Chili due to orography (Lapere et al., 2021).

4. Conclusions

In this study we patch together a global inventory and local data of anthropogenic emissions to obtain an inventory suitable for urban-scale air-quality over the city of Marrakech, Morocco. Comparing simulation results against in-situ NO2, PM10 and ozone observations as well as remote-sensing (AERONET et Terra/Aqua satellite) AOD measurements we show that model results are significantly improved when this new, local inventory is used instead of the global anthropogenic emission CAMS inventory. For particle concentrations we showed that the CAMS inventory underestimates significantly the primary organic particles at the urban location, suggesting omissions in residential emissions. We however, observe an underestimation of particulate matter concentrations at the rural location during wintertime. Transport of dust from the Sahara Desert being rare in wintertime, this underestimation has been attributed to the omission of local dust emissions over the arid rural area in the model. We also note that emissions from agriculture have been spatially distributed in the study domain based on the population density. Energy consumption in the agriculture sector in Morocco is dominated by fossil fuels, with butane/propane representing the 46% of the energy mix of the sector (Raïs et al., 2016). Butane/propane gases being granted from the state for domestic use, the demand of these gases is allocated to the population density. This assumption may be accurate for the emission of gases from the agriculture sector but may misplace particle emissions. A separation in the methodology of the spatial allocation of the SNAP 10 (agriculture) emissions between gases and particle emissions may improve model results at the rural areas. We showed that the accounting for the feedback of aerosols on meteorology through the online coupling of CHIMERE with WRF does not improve model results. The atmosphere of the simulation domain is rich in suspended dust particles in summertime. These particles absorb the long-wave radiation and heat the surrounding atmosphere. We suggest that this temperature increase may be the reason why ozone formation is enhanced in the online simulations leading to a large positive bias.

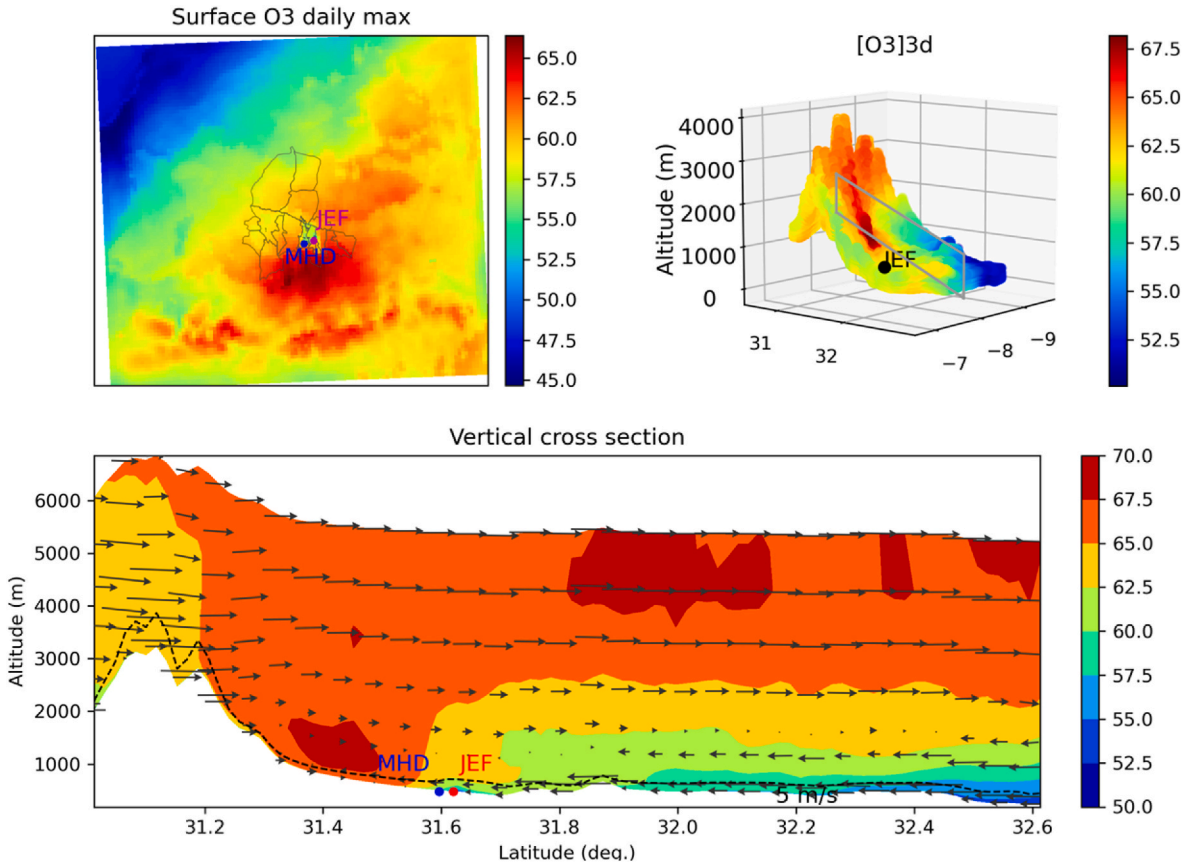

Fig. 8. (Top left) Map of summertime-averaged (July and August) daily maximum surface ozone concentrations (ppb) over the CHIMERE simulation domain. (Top right) 3D scatter plot of ozone concentrations in the first five model vertical layers. The grey rectangle defines the boundaries of the vertical transect of the bottom panel. The Atlas range is shown at the south of the domain. (Bottom) Ozone concentrations in the 12-model layer vertical transect along the upwind-downwind trajectory from the polluted urban center to the Atlas range cutting through the 3D ozone plume. Wind vectors are plotted for different model vertical layers (black arrows), the atmospheric boundary layer is represented with the black dotted line and the location of the urban (JEF) and rural (MHD) monitor sites are given with the red and blue circles respectively. (For interpretation of the references to colour in this figure legend, the reader is referred to the Web version of this article.)

However, more thorough sensitivity studies should be done to confirm this hypothesis.

CRediT authorship contribution statement

Lamiae Saidi: Data collection, spatialiazation of the emission fluxes, part of the simulations, part of the data analysis, Data curation, Formal analysis, Writing – original draft. **Myrto Valari:** part of model simulations, part of data analysis, reviewing and finalizing the final submitted manuscript, Writing – review & editing, Formal analysis. **Jamal Ouarzazi:** Data collection, reviewing and discussion, Writing – review & editing, Data curation.

Declaration of competing interest

The authors declare that they have no known competing financial interests or personal relationships that could have appeared to influence the work reported in this paper.

Data availability

Data will be made available on request.

Acknowledgments

This work was realized within a thesis of the International Doctorate Program (PDI) and financed by the IRD-Marseille. We thank Pr. Cambier, Pr. Ait Babram for their joint supervision. We gratefully acknowledge the contribution of the Moroccan Ministry of Environment, Mines, and Sustainable Energy (MEMSD) for providing Marrakech's 2013 emission inventory. This work was performed using HPC resources from GENCI TGCC (project no. A0050110274).

Appendix A. Supplementary data

Supplementary data to this article can be found online at https://doi.org/10.1016/j.atmosenv.2022.119445.

References

Alfaro, S.C., Gomes, L., 2001. Modeling Mineral Aerosol Production by Wind Erosion: Emission Intensities and Aerosol Size Distributions in Source Areas, vol. 106, pp. 18075–18084. https://doi.org/10.1029/2000JD900339.

Basart, S., Pérez, C., Nickovic, S., Cuevas, E., Baldasano, J., 2012. Development and evaluation of the BSC-DREAM8b dust regional model over Northern Africa. Mediterran. Middle East. 64, 18539 https://doi.org/10.3402/tellusb.v64i0.18539.

Bouet, C., Cautenet, G., Washington, R., Todd, M.C., Laurent, B., Marticorena, B., Bergametti, G., 2007. Mesoscale Modeling of Aeolian Dust Emission during the BoDEx 2005 Experiment, vol. 34. https://doi.org/10.1029/2006GL029184.

Briant, R., Tuccella, P., Deroubaix, A., Khvorostyanov, D., Menut, L., Mailler, S., Turquety, S., 2017. Aerosol–radiation interaction modelling using online coupling between the WRF 3.7.1 meteorological model and the CHIMERE 2016 chemistry-transport model. In: through the OASIS3-MCT coupler, 10, pp. 927–944. https://doi.org/10.5194/gmd-10-927-2017.

Carvalho, H., 2016. The air we breathe: differentials in global air quality monitoring. Lancet Respir. Med. 4, 603–605. https://doi.org/10.1016/S2213-2600(16)30180-1.

Croitoru, L., Sarraf, M., 2017. Estimating the health cost of air pollution: the case of Morocco, 08, 1087. https://doi.org/10.4236/jep.2017.810069.

Emery, C., Liu, Z., Russell, A.G., Odman, M.T., Yarwood, G., Kumar, N., 2017. Recommendations on Statistics and Benchmarks to Assess Photochemical Model Performance, vol. 67, pp. 582–598. https://doi.org/10.1080/10962247.2016.1265027.

Gama, C., Pio, C., Monteiro, A., Russo, M., Fernandes, A.P., Borrego, C., Baldasano, J.M., Tchepel, O., 2020. Comparison of Methodologies for Assessing Desert Dust Contribution to Regional PM10 and PM2.5 Levels: A One-Year Study over Portugal, vol. 11, p. 134. https://doi.org/10.3390/atmos11020134.

Giannadaki, D., Pozzer, A., Lelieveld, J., 2014. Modeled global effects of airborne desert dust on air quality and premature mortality. Atmos. Chem. Phys. 14, 957–968. https://doi.org/10.5194/acp-14-957-2014.

Ginoux, P., Prospero, J., Torres, O., Chin, M., 2004. Long-term simulation of global dust distribution with the GOCART model: correlation with North Atlantic Oscillation. Environ. Model. Software 19, 113–128. https://doi.org/10.1016/S1364-8152(03)00114-2.

Granier, C., Darras, S., Denier van der Gon, H., Doubalova, J., Elguindi, N., Galle, B., Gauss, M., Guevara, M., Jalkanen, J.-P., Kuenen, J., Liousse, C., Quack, B., Simpson, D., Sindelarova, K., 2019. The Copernicus Atmosphere Monitoring Service Global and Regional Emissions. April 2019 version), https://doi.org/doi:10.24380/d0bn-kx16, 2019.

Guenther, A., Karl, T., Harley, P., Wiedinmyer, C., Palmer, P.I., Geron, C., 2006. Estimates of Global Terrestrial Isoprene Emissions Using MEGAN (Model of Emissions of Gases and Aerosols from Nature), vol. 6, pp. 3181–3210. https://doi.org/10.5194/acp-6-3181-2006.

Hauglustaine, D.A., Balkanski, Y., Schulz, M., 2014. A global model simulation of present and future nitrate aerosols and their direct radiative forcing of climate. Atmos. Chem. Phys. 14, 11031–11063. https://doi.org/10.5194/acp-14-11031-2014.

Haustein, K., Pérez García-Pando, C., Baldasano, J., Jorba, O., Basart, S., Miller, R., Janjic, Z., Black, T., Nickovic, S., Todd, M., Washington, R., 2011. Atmospheric dust modeling from meso to global scales with the online NMMB/BSC-Dust model - Part 2: experimental campaigns in Northern Africa. Atmos. Chem. Phys. Discuss. 11, 30273–30331. https://doi.org/10.5194/acpd-11-30273-2011.

Heintzenberg, J., 2009. The SAMUM-1 Experiment over Southern Morocco: Overview and Introduction, vol. 61, pp. 2–11. https://doi.org/10.1111/j.1600-0889.2008.00403.x.

Im, U., Bianconi, R., Solazzo, E., Kioutsioukis, I., Badia, A., Balzarini, A., Baró, R., Bellasio, R., Brunner, D., Chemel, C., 2014. Evaluation of Operational Online-Coupled Regional Air Quality Models over Europe and North America in the Context of AQMEII Phase 2. Part II: Particulate Matter. Atmospheric Environment.

Karyampudi, V.M., Palm, S.P., Reagen, J.A., Fang, H., Grant, W.B., Hoff, R.M., Moulin, C., Pierce, H.F., Torres, O., Browell, E.V., Melfi, S.H., 1999. Validation of the saharan dust plume conceptual model using lidar. Meteosat. ECMWF Data. 80 (2), 1045–1076. https://doi.org/10.1175/1520-0477(1999)080<1045:VOTSDP>2.0.CO.

Kong, X., Forkel, R., Sokhi, R.S., Suppan, P., Baklanov, A., Gauss, M., Brunner, D., Barò, R., Balzarini, A., Chemel, C., Curci, G., Jiménez-Guerrero, P., Hirtl, M., Honzak, L., Im, U., Pérez, J.L., Pirovano, G., San Jose, R., Schlünzen, K.H., Tsegas, G., Tuccella, P., Werhahn, J., Žabkar, R., Galmarini, S., 2015. Analysis of meteorology–chemistry interactions during air pollution episodes using online coupled models within AQMEII phase-2. Atmos. Environ. 115, 527–540. https://doi.org/10.1016/j.atmosenv.2014.09.020.

Lapere, R., Menut, L., Mailler, S., Huneeus, N., 2021. Seasonal Variation in Atmospheric Pollutants Transport in Central Chile: Dynamics and Consequences, vol. 21, pp. 6431–6454. https://doi.org/10.5194/acp-21-6431-2021.

de Longueville, F., Ozer, P., Doumbia, S., Henry, S., 2013. Desert dust impacts on human health: an alarming worldwide reality and a need for studies in West Africa. Int. J. Biometeorol. 57, 1–19. https://doi.org/10.1007/s00484-012-0541-y.

Marticorena, B., Bergametti, G., 1995. Modeling the atmospheric dust cycle: 1. Design. Soil. Derive. Dust. Emission Scheme. 100, 16415–16430. https://doi.org/10.1029/95JD00690.

Mazzeo, A., Huneeus, N., Ordoñez, C., Orfanoz-Cheuquelaf, A., Menut, L., Mailler, S., Valari, M., Denier van der Gon, H., Gallardo, L., Muñoz, R., Donoso, R., Galleguillos, M., Osses, M., Tolvett, S., 2018. Impact of residential combustion and transport emissions on air pollution in Santiago during winter. Atmos. Environ. 190, 195–208. https://doi.org/10.1016/j.atmosenv.2018.06.043.

Mazzeo, A., Burrow, M., Quinn, A., Marais, E.A., Singh, A., Ng'ang'a, D., Gatari, M.J., Pope, F.D., 2022. Evaluation of WRF-CHIMERE Coupled Models for the Simulation of PM2.5 in Large East African Urban Conurbations, vols. 1–31. https://doi.org/10.5194/acp-2021-552.

Menut, L., Schmechtig, C., Marticorena, B., 2005. Sensitivity of the Sandblasting Flux Calculations to the Soil Size Distribution Accuracy, vol. 22, pp. 1875–1884. https://doi.org/10.1175/JTECH1825.1.

Menut, L., Flamant, C., Turquety, S., Deroubaix, A., Chazette, P., Meynadier, R., 2018. Impact of Biomass Burning on Pollutant Surface Concentrations in Megacities of the Gulf of Guinea, vol. 18, pp. 2687–2707. https://doi.org/10.5194/acp-18-2687-2018.

Menut, L., Bessagnet, B., Briant, R., Cholakian, A., Couvidat, F., Mailler, S., Pennel, R., Siour, G., Tuccella, P., Turquety, S., Valari, M., 2021. The CHIMERE V2020r1 Online Chemistry-Transport Model, pp. 1–50. https://doi.org/10.5194/gmd-2021-96.

Ministry of Transport, 2013. Logistics and Water Equipment: Traffic Counting Statistics, 2013.

Monahan, E.C., Spiel, D.E., Davidson, K.L., 1986. A model of marine aerosol generation via whitecaps and wave disruption. In: Monahan, E.C., Niocaill, G.M. (Eds.), Oceanic Whitecaps: and Their Role in Air-Sea Exchange Processes. Springer Netherlands, Dordrecht, pp. 167–174. https://doi.org/10.1007/978-94-009-4668-2_16.

Morman, S.A., Plumlee, G.S., 2013. The role of airborne mineral dusts in human disease. Aeolian Res. 9, 203–212. https://doi.org/10.1016/j.aeolia.2012.12.001.

Moroccan Ministry of Environment, 2018. Mines, and Sustainable Energy: Étude pour la mise en place de systèmes de modélisation de la dispersion des polluants atmosphériques PHASE 3 : Actualisation de l'inventaire des émissions atmosphériques et réalisation de la modélisation de la dispersion des polluants atmosphériques. Ville de Marrakech.

Raïs, R., Faysse, N., Lejars, C., 2016. Impacts d'un changement de politiques énergétiques sur les exploitations irriguées : éclairage sur la base d'un échantillon d'exploitations dans le Saiss (Maroc), vol. 4.

Ridley, D.A., Heald, C.L., Ford, B., 2012. North African Dust Export and Deposition: A Satellite and Model Perspective, vol. 117. https://doi.org/10.1029/2011JD016794.

Tuccella, P., Menut, L., Briant, R., Deroubaix, A., Khvorostyanov, D., Mailler, S., Siour, G., Turquety, S., 2019. Implementation of aerosol-cloud interaction within WRF-CHIMERE online coupled model: evaluation and investigation of the indirect

radiative effect from anthropogenic emission. Reduct. Benelux Union. 10, 20. https://doi.org/10.3390/atmos10010020.
Washington, R., Todd, M.C., Engelstaedter, S., Mbainayel, S., Mitchell, F., 2006. Dust and the Low-Level Circulation over the Bodélé Depression, vol. 111. Observations from BoDEx, Chad. https://doi.org/10.1029/2005JD006502, 2005.
World Bank, 2020. The Global Cost of Ambient PM25 Air Pollution.
World Health Organization, 2006. Air Quality Guidelines: Global Update 2005: Particulate Matter, Ozone, Nitrogen Dioxide, and Sulfur Dioxide. World Health Organization, Copenhagen, Denmark, p. 484.
World Health Organization, 2016. Ambient Air Pollution: a Global Assessment of Exposure and Burden of Disease. World Health Organization, p. 121.